Study on the Mixing Performance of Micro Optical Rotor by CFD*

Yoshifumi OGAMI**, Ken NISHIKAWA*** and Hiroo UKITA****

The mixing efficiency of an optical micro rotor designed to be used as a part of the Micro Total Analysis Systems has been studied using Computational Fluid Dynamics. It is found that the mixing efficiency due to convection by the rotor depends on the ratio of the circumferential speed of the rotor to the inlet speed of the fluids, and the efficiency due to the diffusion of the fluids depends on the ratio of the diffusion coefficient of the fluids to the inlet speed. A multiplier effect due to convection by the rotor and diffusion of the fluids on the mixing performance is observed. The results obtained in this study can be used for designing more effective optical micro rotor systems.

Key Words: Micro Total Analysis Systems, Turbulent Mixing, Computational Fluid Dynamics, Diffusion, Micromachine

1. Introduction

Recently, the research regarding μTAS (Micro Total Analysis Systems)[1] has been increasing; this system integrates the functions of organic syntheses, chemical analysis, etc. on a single chip using microfabrication technologies. Further, a microchannel is fabricated on a glass or silicon substrate, where a chemical synthesis reaction, antigen-antibody reaction, etc. are analyzed. The following are the advantages of μTAS:

(1) Due to its small size and light weight, it can be carried or used in the field.

(2) The amount of liquid reagent used can be reduced and the temperature can be accurately controlled.

(3) Multiple reactions can be observed and analyzed simultaneously.

However, in the microscale fluid region, the Reynolds number reduces to such an extent that it interferes with the onset of turbulence. Therefore, it becomes difficult to mix the liquid reagents, which is essential for an effective reaction. In order to accelerate the mixing process, the following methods are suggested and their effectiveness is reported.

1. Designing the channels

a) Prepare several outlets of the liquid reagents (Ref. (1), p.73)

b) Set the channel in a zigzag shape (Ref. (1), p.141)

c) Divide and combine the fluid flows (Ref. (1), p.237), (Ref. (2)).

2. Pulsating the liquid reagents[3]

Contrary to the abovementioned ideas, a micro optical rotor system has been suggested[4],[5]. This device traps and rotates a small transparent element like a screw by the optical tweezers technique[6]. The fluid mixing process can be accelerated with the help of this rotor placed in a microchannel. Since optical energy is the driving force for this rotor, remote operation is possible and a roller bearing is not required for the rotor.

In order to design the micro optical rotor system that utilizes these advantages, it is necessary to clarify the conditions for the proper values of parameters such as (1) rotation speed of the rotor, (2) diffusion coefficient of the liquid reagents, (3) inlet velocity of the liquid reagents, and (4) size of the device in order to sufficiently accelerate the mixing process. Moreover, it is desirable to provide the conditions for versatility that can deal with various liquid reagents.

In this study, in order to provide a guideline for designing the micro optical rotor system, the relation be-

* Received 3rd March, 2006 (No. 05-0116). Japanese Original: Trans. Jpn. Soc. Mech. Eng., Vol.71, No.710, B (2005), pp.2434–2441 (Received 3rd February, 2005)

** Department of Mechanical Engineering, Ritsumeikan University, 1–1–1 Nojihigashi, Kusatsu, Shiga 525–8577, Japan. E-mail: y_ogami@cfd.ritsumei.ac.jp

*** Mitsubishi Electric, 5–1–14 Yadaminami, Higashi-ku, Nagoya, Aichi 461–8670, Japan

**** Department of Photonics, Ritsumeikan University, 1–1–1 Nojihigashi, Kusatsu, Shiga 525–8577, Japan. E-mail: ukita@se.ritsumei.ac.jp

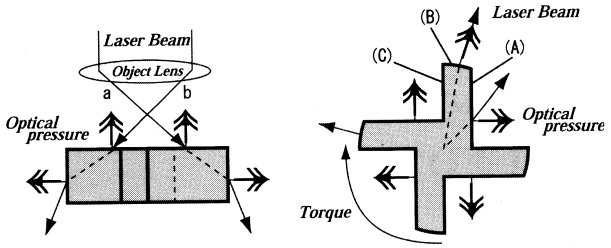

(a) Side view (b) Top view

Fig. 1 Principle of optical trapping and rotation

tween the mixing effect of this rotor and the abovementioned conditions is clarified by computational fluid dynamics (CFD).

Although the optical energy is considered as the driving force of the rotor in this study, our results will be applied to systems with a magnet-driven rotor, motor-driven rotor, etc.

2. Micro Optical Rotor

This chapter explains the principles of trapping and rotating the micro optical rotor that utilizes optical energy as its driving force, as mentioned in chapter 1.

As shown in Fig. 1 (a), the laser beams "a" and "b" focused on by the objective lens are refracted while entering the surface of the four-blade rotor. The change in momentum due to this refraction results in a force on the surface along the vertical direction, which acts as the "optical pressure." The rotor is trapped at a position where the resultant force due to the optical pressure, gravity, and buoyancy acting on the rotor are balanced. Similarly, the optical pressure is generated when the beams that pass through the rotor body emerge from the rotor surfaces; this represents the torque of the rotor.

As shown in Fig. 1 (b), surfaces (A), (B), and (C) on one of the blades of the rotor are considered. The beam emerging from surface (A) generates the optical pressure acting along the vertical direction on this surface at the time of refraction, resulting in the generation of a clockwise rotation torque. Since surface (B) is a part of the circumference, the optical pressure acting vertically on this surface will not generate a rotation torque. Further, an optical pressure is not generated on surface (C) as the beam does not emerge from this surface. Therefore, the rotation torque acting on this rotor is due to the optical pressure on the four sides of the blades that correspond to surface (A). The rotor is rotated clockwise due to this torque.

3. Numerical Methods and Results

3.1 Microchannel

Figure 2 shows the shape and dimensions of the optical micro rotor used in this research. The diameter of the rotor is 20 μm, and the width and height of each blade are 4 μm and 10 μm, respectively. Figure 3 shows a Y-shaped

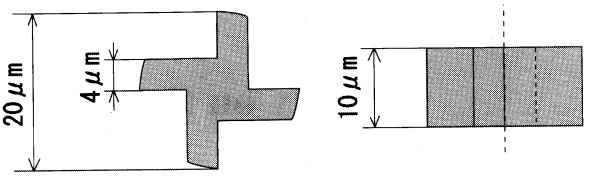

Fig. 2 Optical micro-rotor

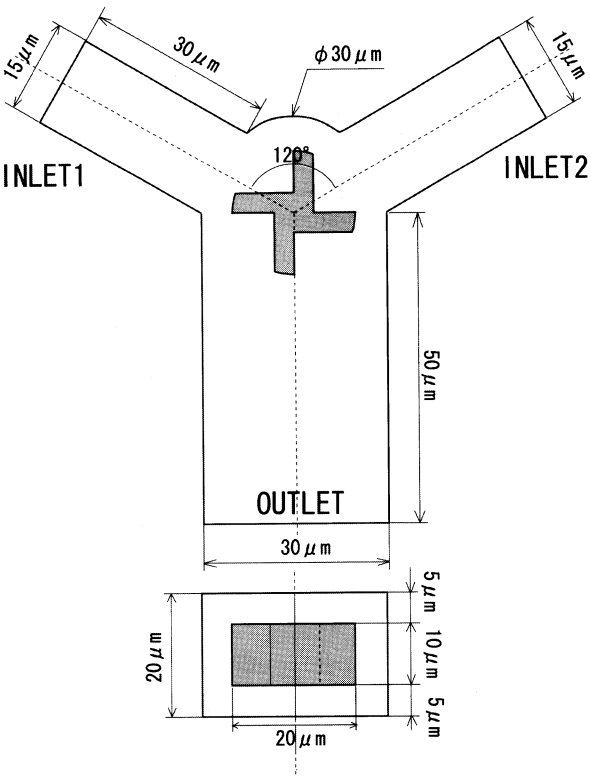

Fig. 3 Y-shaped micro-channel and rotor

microchannel used in our calculations. It is assumed that the rotor is trapped and rotating at the center of the channel. The flows of the two liquid reagents from INLET1 and INLET2 are stirred and mixed by the rotor, and the mixed liquid reagent flows out from the OUTLET.

Figure 4 shows the computational grids of the channel. The grids of the rotor exhibit an axisymmetric structure such that the technique of rotational grids can be used. The number of grids used for the inlets is 12×20, that for the outlet is 30×20; further, the total number of the grids is around 70 000. The mixing rate (later provided by Eq. (4)) obtained by the preliminary calculation with approximately 120 000 grids differs by only 0.3% from the rate obtained with 70 000 grids. Therefore, the results from 70 000 grids are considered to be sufficiently accurate.

3.2 Equations and numerical method

The following equations are considered: the continuity equation (1), momentum equation (2), and transport equation of concentration c (3) in three dimensions, where the moving velocity vector $\dot{\boldsymbol{x}}$ of the rotor is incorporated.

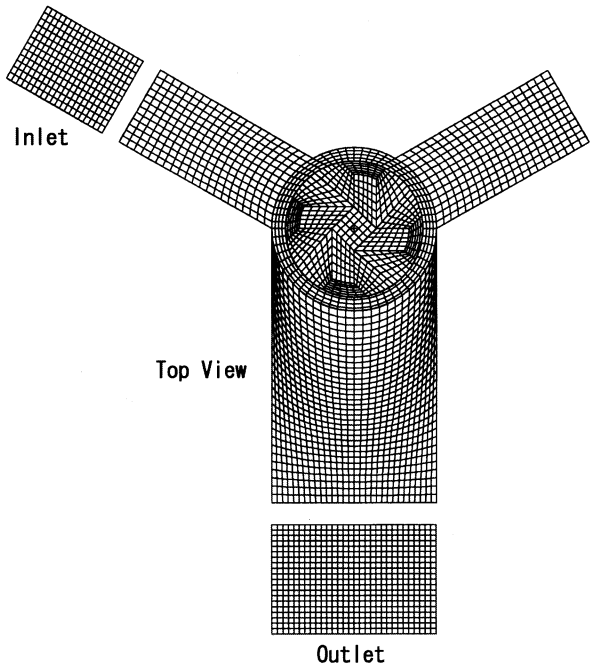

Fig. 4 Grid-system of Y-shaped micro-channel and rotor

The parameters $\boldsymbol{u}$, ρ, p, and μ denote the velocity vector, density, pressure and viscosity of the fluid, respectively. D denotes the interdiffusion coefficient for the two liquid reagents. Knudsen diffusion is not considered in this study.

$$\nabla\cdot(\boldsymbol{u}-\dot{\boldsymbol{x}})=0 \tag{1}$$

$$\frac{\partial \boldsymbol{u}}{\partial t}+\{(\boldsymbol{u}-\dot{\boldsymbol{x}})\cdot\nabla\}\boldsymbol{u}=-\frac{1}{\rho}\nabla p+\mu\nabla^2\boldsymbol{u} \tag{2}$$

$$\frac{\partial c}{\partial t}+(\boldsymbol{u}\cdot\nabla)c=D\nabla^2 c \tag{3}$$

With regard to the discretization of these equations in space, the central difference in the second-order accuracy (the upwind difference in the first-order accuracy for the convection term) is used. With regard to the discretization in time, the implicit method in the first-order accuracy is used. Further, the SIMPLE[7] method is used to calculate the pressure.

The computational grid system that contains the rotor is rotated at a constant angular velocity; further, at the interface between the rotational and non-rotational grids, the numerical values are exchanged using the interpolation method. In order to determine the time step Δt, the stability condition is set according to the grid width, rotation speed of the rotor, and inlet velocity of the fluid. The range of the time step varies between 0.005 s and 0.1 s depending on the stability condition. It is assumed that convergence has been achieved when the order of the relative residual reduces to 10^{-6} at each time step.

The physical properties of the fluids are the same as those of water at 293 K (i.e., density $\rho=9.978\times10^2$ kg/m^3 and viscosity $\mu=1.024\times10^{-3}$ Pa·s). The order of the Reynolds number in our calculation is $1\times10^{-4}\sim1\times10^{-2}$, and the flow is considered to be laminar.

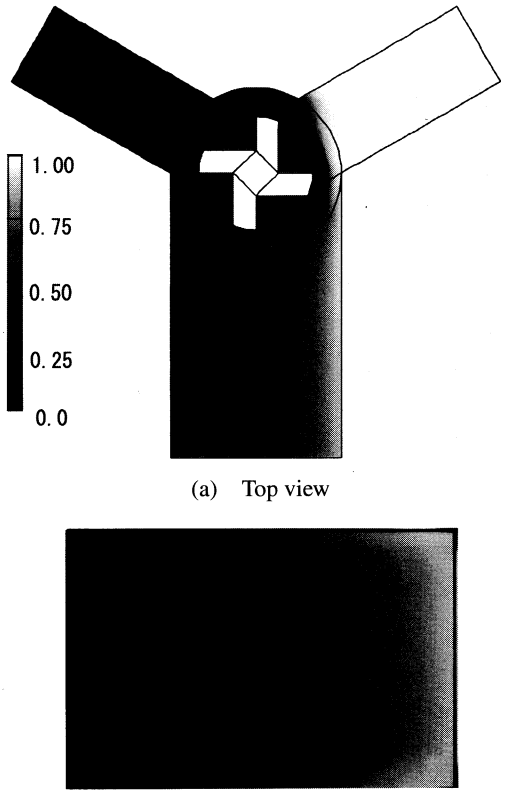

(a) Top view

(b) Outlet

Fig. 5 Concentration distribution (400 rpm, 33.33 μm/s)

3.3 Mixing effect due to convection by rotor

First, in order to clarify the accuracy of our calculation and the mixing effect of convection caused by the rotor, we set the interdiffusion coefficient D to 0.

Figure 5 demonstrates how the liquid reagent from INLET1 (shown in black) and that from INLET2 (shown in white) are stirred and mixed by the rotor at a rotation speed $\omega=400$ rpm and at an inlet velocity of liquid reagents $u=33.33$ μm/s. In this figure, the gray level indicates the volume fraction (white: 1, black: 0) in the steady state, which corresponds to the concentration of the mixed liquid reagent. Due to the effect of the rotor, the color in the channel has transformed to gray except near the channel sidewalls.

With regard to comparison, Fig. 6 shows the results when the rotation speed of the rotor is set to 0. The inlet velocity is set to 33.33 μm/s. Since the stirring effect or mixing of the two fluids is absent, the joint area in which the color transforms to gray is narrow. Although the color-coding is supposed to be performed only using the colors black and white, a volume fraction other than 0 or 1 inevitably exists because of the numerical error due to the use of a finite grid size (i.e., discretization error).

In order to quantitatively evaluate the mixing effect,

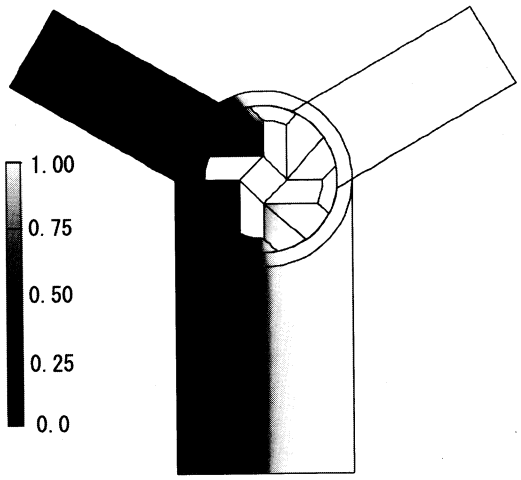

(a) Top view

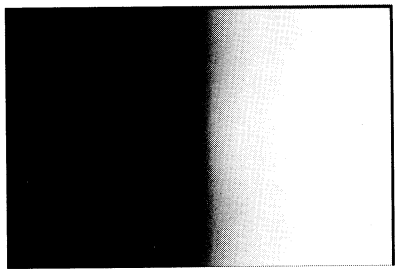

(b) Outlet

Fig. 6 Concentration distribution (0 rpm, 33.33 μm/s)

the mixing rate M defined by the following formula is used.

$$M = 1 - \frac{1}{\bar{C}} \sqrt{\frac{\sum (C_i - 0.5)^2}{N}} \tag{4}$$

In this case, C_i is the volume fraction at the ith nodal point on the surface of the OUTLET, N is the total number of the grids on this surface (i.e., 600), and $\bar{C}$ is the average value of volume fraction defined as

$$\bar{C} = \frac{\sum C_i}{N} \tag{5}$$

In the absence of a mixture, M becomes zero; when the mixing process completes, it changes to 1.

Figure 7 shows the variations in M with time at four different rotation speeds. In all the cases, the inlet velocity is set to 33.33 μm/s. After the time during which the fluid from the inlet reaches the outlet elapses, the mixing rate increases and reaches each of the steady values, as shown in the figure. The mixing rate at the steady state also increases with the rotation speed of the rotor; thus, the mixing effect of the rotor is clearly shown. Although the mixing rate should be zero when the rotation speed of the rotor is zero, the rate inevitably reduces to a finite value of 0.066 9 as a result of the previously mentioned discretization error. Therefore, errors of this order are inherent in our calculations.

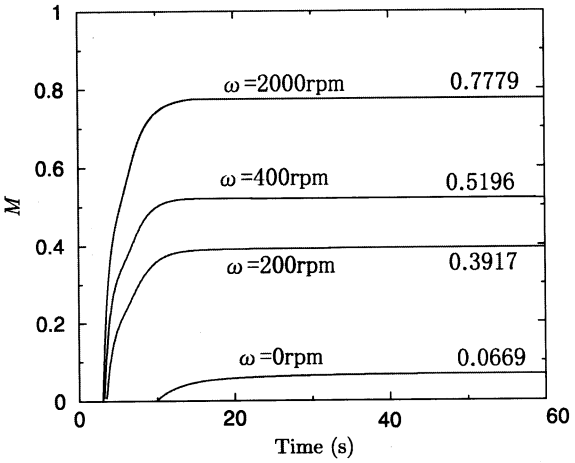

Fig. 7 Time history of mixing rate at various rotation speeds at inlet velocity 33.33 μm/s

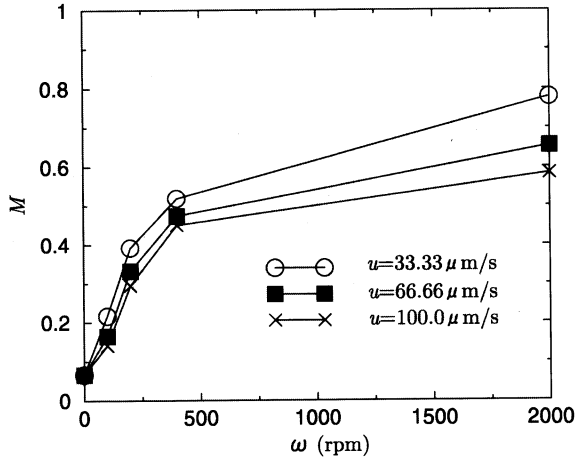

Fig. 8 Mixing rate at various rotation speeds and inlet velocities at $D = 0$

Figure 8 shows the variations in M in the steady state for three different inlet velocities, namely, 33.33, 66.66, and 100.0 μm/s when the rotation speed of the rotor ω is varied from 0 to 200 rpm. The mixing rate increases with the rotation speed, which demonstrates the mixing effect of the rotor. At the same rotation speed, the mixing rate is greater when the inlet velocity is lower. This is because the time for stirring the fluid by the rotor increases at a smaller inlet velocity. Moreover, at the rotation speed of zero, the mixing rate is always 0.066 9, irrespective of the inlet velocity. This indicates that the numerical errors, except the previously mentioned discretization error, are sufficiently small.

Figure 9 shows the mixing rate M with the dimensionless rotation speed $\pi R\omega/(30u)$. The radius of the rotor is $R = 10$ μm. In this figure, the data of Fig. 8 are indicated by the symbols ○, ■, and ×, and the results of the additional calculations are indicated by △. It is observed that, irrespective of the inlet velocities, the calculated values are approximated by a single curve (solid line). Therefore, it

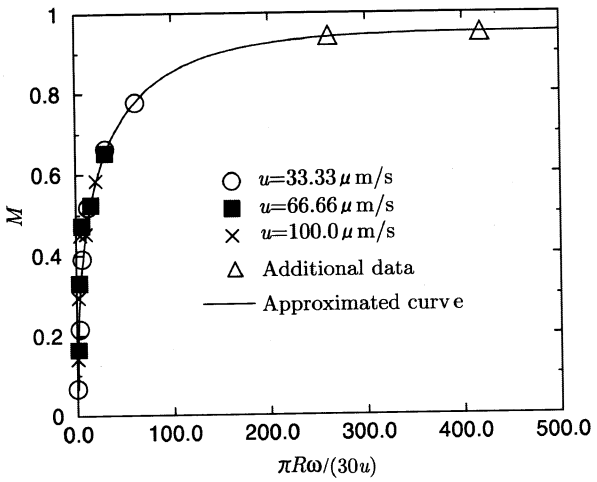

Fig. 9 Similarity of mixing rate at $D=0$

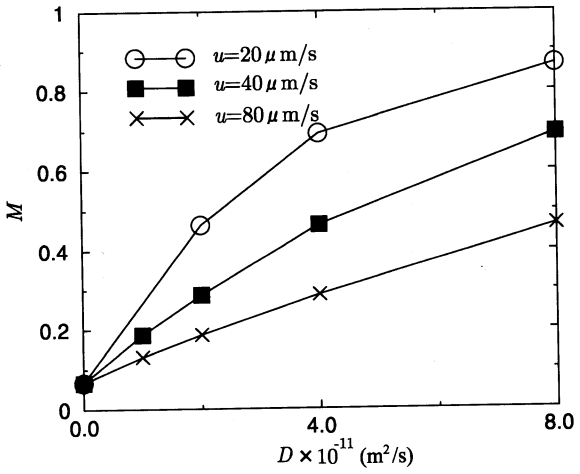

Fig. 10 Mixing rate at various interdiffusion coefficients and inlet velocities at $\omega=0$

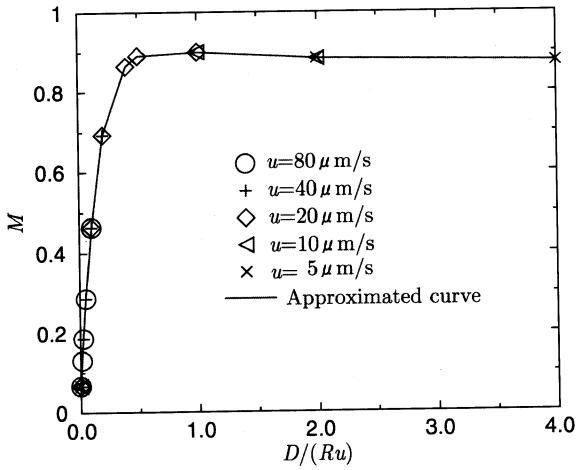

Fig. 11 Similarity of mixing rate at $\omega=0$

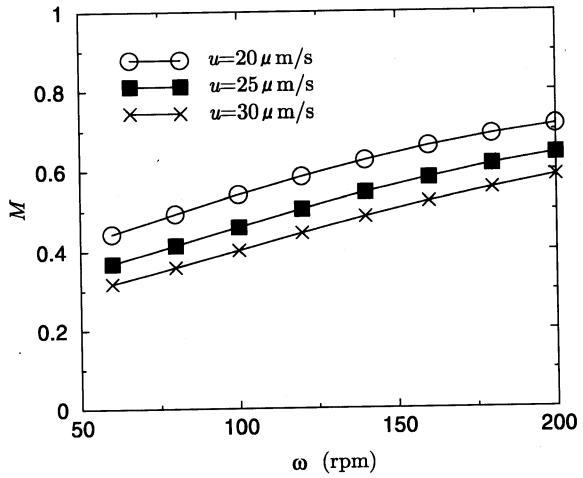

Fig. 12 Mixing rate at various rotation speeds and inlet velocities at $D=1\times10^{-11}$

is evident that there exists a similarity—the mixing rate is the same at the same values of $\pi R\omega/(30u)$ for different inlet velocities. As will be mentioned in the next section, M depends on the ratio of the interdiffusion coefficient D and the inlet velocity u, i.e., D/u. The effect of convective mixing by the rotor is similar to the effect by diffusion, and it can be related to this effect. Further, the rotation speed of the rotor can be converted into the interdiffusion coefficient, as will be explained in chapter 4.

3.4 Mixing effect due to diffusion of fluids

In this section, in order to study the effect of diffusive mixing of fluids, the convection effect of the rotor is excluded by setting the rotation speed ω of the rotor equal to zero.

Figure 10 shows the mixing rate M and the interdiffusion coefficient D at the inlet velocities of u = 20, 40 and 80 μm/s. D is set between 0 and 8×10^{-11} m^2/s. For example, the interdiffusion coefficient of hemoglobin in 20°C water is 6.9×10^{-11} m^2/s[8]. As shown in this figure, M increases with D. Further, it increases with a decrease in the inlet velocity because the transit time of the fluids flowing from the inlet to the outlet increases with this decrease; consequently, the effect of diffusion becomes more evident.

In Fig. 11, the horizontal axis is nondimensionalized as $D/(Ru)$; further, the data in Fig. 10 and the results of the additional calculations are shown. Furthermore, for the same value of $D/(Ru)$, M takes almost the same value even when the inlet velocity and interdiffusion coefficient are different. This is because the diffusion of fluids depends on $\sqrt{Dt}$ (namely, $\sqrt{D/u}$ or D/u).

3.5 General case

This section considers the mixture obtained by the convective effect of the rotor as well as by the diffusion effect of the fluids. In Fig. 12, the mixing rate is plotted for a constant interdiffusion coefficient $D=1\times10^{-11}$ m^2/s with three inlet velocities, namely, 20, 25 and 30 μm/s. In a manner similar to the one observed in Fig. 10, the mixing rate increases with the rotation speed of the rotor and

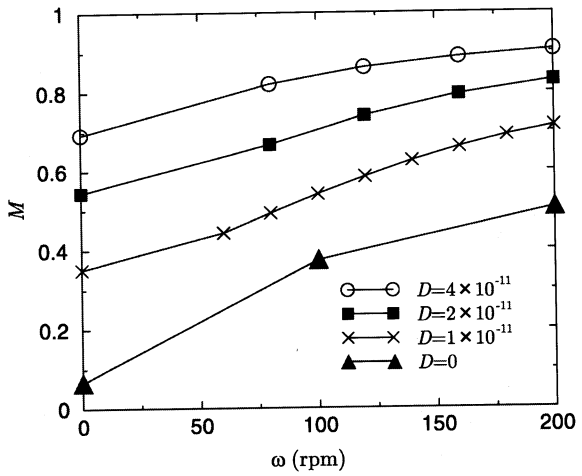

Fig. 13 Mixing rate at various rotation speeds and diffusion coefficients at $u = 20\,\mu$m/s

with a decrease in the inlet velocity.

Figure 13 shows the results for a constant inlet velocity $u = 20\,\mu$m/s when D assumes four values: 0, 1×10^{-11}, 2×10^{-11} and 4×10^{-11} m^2/s. At a constant rotation speed, it is observed that the mixing rate increases with the interdiffusion coefficient and for a constant interdiffusion coefficient, this rate increases with the rotation speed. Chapter 4 provides a detailed discussion on the convection mixture and diffusion mixture.

3.6 Effect of size

In order to obtain the same mixing rates as shown in Figs. 9 and 11 for an n-fold increase in the size of the device, it is necessary to increase the inlet velocity by n times and the interdiffusion coefficient by n^2 times with the same rotation speed. This is because the transit time of the fluid from the inlet to the outlet is the same (because both the device size and the inlet velocity are n times larger); further, for the mixed area to spread n times wider due to diffusion within this time period, the interdiffusion coefficient needs to be greater by n^2 times.

In order to verify this, the calculations are conducted at the three different rotation speeds (200, 400 and 800 rpm) for n = 10; in other words, the interdiffusion coefficient and inlet velocity are 100 times and 10 times greater, respectively, than those of the basic model shown in Fig. 3. The results are summarized in Table 1. For all the cases, the mixing rates of the ten-fold model are in good agreement with those of the basic model; therefore, the relevance of the above discussion is confirmed.

Further, when the size of the device increases n times, the parameter on the horizontal axis in Fig. 9 remains the same, that is, $(nR)\pi\omega/30/(nu) = \pi R\omega/(30u)$; this is also the case for Fig. 11, that is, $n^2D/(nR)/(nu) = D/(Ru)$. This indicates that the results in Figs. 9 and 11 are valid even for devices with different sizes.

Table 1 Similarity of mixing rate between two models

Basic model				Tenfold model			
ω rpm	D m^2/s	u μm/s	M	ω rpm	D m^2/s	u μm/s	M
800	2×10^{-11}	40	0.7825	800	200×10^{-11}	400	0.7799
400	4	40	0.8009	400	400	400	0.8010
200	8	20	0.9126	200	800	200	0.9126

4. Discussion

First, the effects of convective mixing by the rotor and diffusive mixing of the fluids are discussed.

By considering that the diffusion coefficient is proportional to the speed and mean free path of the molecules in random motion, the fluid particles rotated by the rotor are forcefully imparted a speed and displacement, which produces a similarity between both the mixing effects. This is why the mixing rate by convective mixing depends on $\pi R\omega/(30u)$, similar to the manner in which this rate depends on $D/(Ru)$ by diffusive mixing.

In order to study the quantitative relation between the effects of convective mixing by the rotor and the diffusive mixing of the fluids, the parameter on the horizontal axis in Fig. 14 is modified to $D/(Ru)+\pi R\omega/(30u)/191$. This is obtained by shrinking the horizontal axis in Fig. 11 by 1/191 such that the approximated curves in Figs. 9 and 11 correspond to each other (namely, the root-mean-square of the difference between the two curves is minimized), particularly in the region where a significant variation in M is observed (e.g., $D/(Ru) < 0.5$ in Fig. 11). In Fig. 14, the approximated curve obtained in Fig. 9 is indicated by a solid line and that obtained in Fig. 11 by a long dashed line. Although these curves do not completely agree with each other, a rough estimation of the diffusion effect by the rotation speed ω (rpm) is given as follows:

$$D_\omega = \frac{\pi R^2 \omega}{5\,730}\ (\mathrm{m^2/s}) \qquad (6)$$

For example, the diffusion coefficient of the rotor at ω = 800 (rpm) is calculated as $D = 4.39\times10^{-11}$ (m^2/s).

In Fig. 14, the mixing rates with nonzero values of D and ω are plotted using symbols ●, □, and ×. These results can be approximated by a single curve (short dashed line); although a few noticeable deviations exist, a similarity is observed.

Interestingly, a multiplier effect due to convective mixing by the rotor and diffusive mixing of the fluids is observed. This is confirmed by the fact that in the region with large mixing rates (for example, $M > 0.6$), these rates with nonzero values of D and ω (symbols ●, □, and ×) are greater than the rates obtained when $D = 0$ (solid line) and $\omega = 0$ (broken line). The parameter $D/(Ru)+\pi R\omega/(30u)/191$ on the horizontal axis is regarded as a similarity parameter, and the mixing rate is the

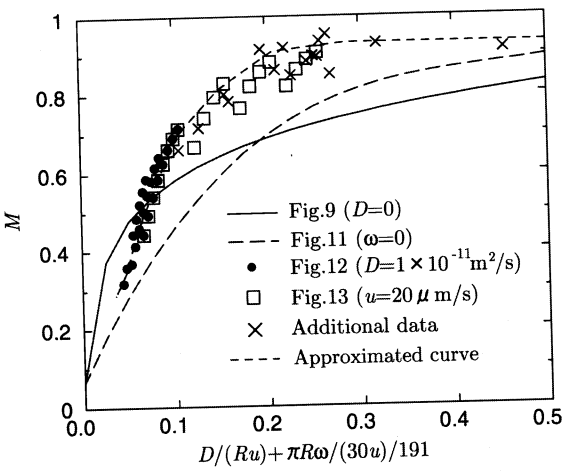

Fig. 14 Multiplier effect of mixing rate

Table 2 Multiplier effect

$a = D/(Ru)$, $b = \pi R\omega/(30u)/191$

ω rpm	D m^2/s	u μm/s	M	a	b	$a+b$	a/b
800	4.39×10^{-11}	43.86	0.912	0.1	0.1	0.2	1.0
800	0.439	24.12	0.920	0.0182	0.182	0.2	0.1
800	43.9	241.2	0.859	0.182	0.0182	0.2	10.0

same for the same value of this parameter. When the similarity parameter is around 0.2, the mixing rate is almost 0.7 both for only convection ($D = 0$) and only diffusion ($\omega = 0$). However, when D and ω are both nonzero, the mixing rates are greater than 0.7 when the similarity parameter is around 0.2.

In order to observe the multiplier effect, calculations are performed at a constant rotation speed of $\omega =$ 800 (rpm) along with the parameters that satisfy the relation $D/(Ru)+\pi R\omega/(30u)/191 = 0.2$. The results obtained are listed in Table 2, where the relations $a = D/(Ru)$ and $b = R\omega/(30u)/191$ are used. In this table, for the parameters D and μ that are selected to yield $a/b = 0.1$, 1 and 10, the values of M are 0.912, 0.920 and 0.859, respectively. These rates are greater than those with either the convective effect — 0.69 ($D = 0$) — or the diffusive effect — 0.7 ($\omega = 0$); thus, the multiplier effect is confirmed.

As previously mentioned in the Introduction, it is desirable to provide the conditions for versatility that can deal with various liquid reagents. Therefore, a discussion on the versatility of the micro optical rotor system is given below. It is known that the relation between the diffusion time t_D, mixing length L_M, and diffusion coefficient D is given by[9]

$$t_D = \frac{L_M^2}{2D} \tag{7}$$

The mixing length of our device is $L_M = 30$ μm (width of the OUTLET in Fig. 3). The time period within which the liquid reagents from the two inlets meet at the junction and reach the outlet is estimated as 50 μm (channel length) ÷ u (inlet speed). Sufficient diffusion is achieved when this time period is greater than the diffusion time t_D. Therefore, the following condition is obtained for sufficient diffusion:

$$t_D = \frac{L_M^2}{2D} < \frac{50\,(\mu\text{m})}{u}$$
$$u < \frac{100\,(\mu\text{m})D}{L_M^2} \tag{8}$$

Here, the rotor is not considered. The volumetric flow rate Q_D is calculated as

$$Q_D = u\times 30\times 20\,(\mu\text{m})^2 < \frac{200}{3}D\times 10^{-6}\ [\text{m}^3/\text{s}] \tag{9}$$

This indicates that the amount of well-mixed reagent is proportional to the diffusion coefficient; further, a considerable time period is required to obtain a sufficient amount of mixed reagent if the diffusion coefficient of the liquid reagent is small.

However, with convective mixing by the rotor (Eq. (6)), the upper limit of the inlet velocity is increased as follows:

$$u < \frac{100\,(\mu\text{m})}{L_M^2}\left(D + \frac{\pi R^2\omega}{5\,730}\right) \tag{10}$$

Further, the volumetric flow rate Q_{D+C} for this flow is expressed as

$$Q_{D+C} < \frac{200}{3}\left(D + \frac{\pi R^2\omega}{5\,730}\right)\times 10^{-6}\ [\text{m}^3/\text{s}] \tag{11}$$

This indicates that even if the diffusion coefficient is small, a sufficient amount of mixed liquid reagent can be obtained by increasing the rotation speed ω. This eliminates the limitation on the diffusion coefficients of liquid reagents and improves the versatility of the system. For example, the volumetric flow rate of hemoglobin in water at 20°C ($D = 6.9\times10^{-11}$ m^2/s) is $Q_D < 4.6\times10^{-15}$ [m^3/s] without taking into account the effect of the rotor, while it increases to $Q_{D+C} < 7.5\times10^{-15}$ [m^3/s] when the rotation speed of the rotor is $\omega = 800$ rpm.

Finally, the relation between the size of the device and the volumetric flow rate is discussed. In section 3.6, the discussion is based on the various values of the diffusion coefficient and the rotation speed. In this case, we consider of a device that is n-fold in size with constant diffusion coefficient and rotation speed.

In the absence of the rotor, the relation between the diffusion time t_D, the mixing length L_M, the diffusion coefficient D, and the inlet velocity u for the n-fold device is given by

$$t_D = \frac{n^2L_M^2}{2D} < \frac{50n\,(\mu\text{m})}{u}$$
$$u < \frac{100\,(\mu\text{m})D}{nL_M^2} \tag{12}$$

This shows that for a sufficient amount of mixing, the inlet speed has to be $1/n$-th of that in Eq. (8). The volumetric

Table 3 Scaling effect

$D = 1\times10^{-11}$ m^2/s, ω = 800rpm

	u μm/s	Q_{D+C} $\times10^{-15}$m^3/s	M
Basic model	5.984	5.59	0.996
Tenfold model	48.84	2931	0.986

flow rate Q_D is increased n times as compared to that in Eq. (9) as follows:

$$Q_D = u\times 30n\times 20n\,(\mu\text{m})^2 < \frac{200}{3}Dn\times10^{-6}\ [\text{m}^3/\text{s}] \tag{13}$$

Further, by taking into account the effect of the rotor (Eq. (6)), the inlet velocity can be expressed as

$$u < \frac{100\,(\mu\text{m})}{nL_M^2}\left(D+\frac{\pi n^2R^2\omega}{5\,730}\right) \tag{14}$$

and the volumetric flow rate Q_{D+C} as

$$Q_{D+C} < \frac{200}{3}\left(Dn+\frac{\pi R^2\omega}{5\,730}n^3\right)\times10^{-6}\ [\text{m}^3/\text{s}] \tag{15}$$

The diffusion effect term (the first term on the right-hand side of Eq. (15)) is n times greater than that in Eq. (11), while the convective effect term (the second term on the right-hand side of Eq. (15)) is n^3 times greater. Therefore, it is expected that the rotor has a significant effect on the mixing rate.

In order to confirm this effect, calculations are conducted for devices with a basic size and a ten-fold size at $D = 1\times10^{-11}$ m^2/s and $\omega = 800$ rpm with the upper limits of the inlet velocities as defined in Eqs. (10) and (14); the results of these calculations are tabulated in Table 3. The mixing rate is almost one in both the cases, indicating that a sufficient mixing is achieved. The volumetric flow rate for the basic device is 5.59×10^{-15} m^3/s and, as expected, it increases by triple digits to $2\,931\times10^{-15}$ m^3/s for the ten-fold device.

In summary, for a given diffusion coefficient of a liquid reagent and a requested amount of mixed reagents, the size of the device, rotation speed, and inlet velocity of the liquid reagent for a sufficient mixing rate can be determined; thus, a guideline for designing the micro optical rotor system is presented.

5. Conclusion

The mixing efficiency of an optical micro rotor designed to be used as a part of the Micro Total Analysis Systems has been studied using computational fluid dynamics. The results are summarized as follows:

1. The effect of convective mixing by the rotor depends on the ratio of the circumferential speed of the rotor to the inlet speed of the liquid reagent, and the mixing effect of diffusion of the liquid reagent depends on the ratio of the interdiffusion coefficient of the liquid reagents to the inlet speed of the liquid reagents.
2. The rotor at the rotation speed of ω (rpm) corresponds to a diffusion coefficient of $\pi R^2\omega/5\,730$ (m^2/s).
3. The multiplier effect due to convection by the rotor and diffusion of fluids on the mixing performance is observed.
4. In the case of a device that is n-fold in size, the volumetric flow rate of sufficiently mixed fluids as well as the diffusive mixing effect of the fluids increases n-fold, while the convective mixing effect by the rotor increases n^3-fold; therefore, the rotor significantly affects the mixing rate.

The guideline for designing the micro optical rotor system presented in this paper can be applied to systems with magnet-driven or motor-driven rotors.

References

(1) Berg, A. van den and Bergveld, P., Micro Total Analysis Systems, (1995), p.1, Kluwer Academic Publishers.

(2) Hatanaka, O. and Kato, Y., Acceleration of Mixing and Chemical Reaction by Changing the Flow Channel Configuration in a Micro-Fluidic Device, Proceedings of Mechanical Engineering Congress, 2004 Japan, (in Japanese), Vol.2, No.04-1 (2004), pp.113–114.

(3) Shintaku, H., Kawano, S., Kanno, I. and Kotera, H., Micro Liquid Mixing Using Pulsating Flow at Extremely Low Reynolds Numbers, Proceedings of Mechanical Engineering Congress, 2004 Japan, (in Japanese), Vol.2, No.04-1 (2004), pp.67–68.

(4) Ukita, H., Ogami, Y., Tabata, O. and Konishi, S., Microenergy Driven by Optical Pressure, NEDO Project, (in Japanese), (1999), 97S22-002-1.

(5) Ukita, H., Takada, K. and Itoh, Y., Experimental and Theoretical Analyses of Three Dimensional Micro-Flows Generated by an Optical Mixer, Proc. SPIE, Vol.5514 (2004), pp.704–711.

(6) Ukita, H., The Leading Edge of Opt-Mechatronics, (in Japanese), (1995), p.46, Koudansha.

(7) van Doormal, J.P. and Raithby, G.D., Enhancements of the SIMPLE Method for Predicting Incompressible Fluid Flows, Numerical Heat Transfer, Vol.7 (1984), pp.147–163.

(8) Atkins, P.W., Physical Chemistry, (in Japanese), (1993), p.1046, Tokyo-Kagaku-Doujin.

(9) Nguyen, N.T. and Wereley, S.T., Fundamentals and Applications of Microfluidics, (2002), p.387, Artech House.